Evidence

Evidence in Earth Science

RESEARCH ARTICLE

DOI: 10.63221/eies.v1i04.189-207

Highlights:

- ASTER data effectively maps marine carbonate and continental formations in Ganjina-Khuroson.
- New band ratio algorithms improved lithological discrimination.
- Maximum Likelihood Classification achieved over 90% accuracy.
- Field spectra confirmed remote sensing results.

Keywords:

Remote Sensing
ASTER
Tertiary marine carbonate outcrops
Lithological discrimination
Tajik Basin
GRACE

Correspondence to:
climate0793@yandex.com

Citation: Ibodullo Qaraev, Masoud Jafari Shalamzari, Malihe Qaderi, 2025. Reconstructing the Late Cenozoic Retreat of the Proto-Paratethys Sea in the SW Tajik Basin Using Integrated ASTER Mapping and Field Validation. Evidence in Earth Science, 1(04), 189-207.

Manuscript Timeline

Received	October 10, 2025
Revised	November 5, 2025
Accepted	November 17, 2025
Published	November 25, 2025

Academic Editor:

Haoyu Wang

Reconstructing the Late Cenozoic Retreat of the Proto-Paratethys Sea in the SW Tajik Basin Using Integrated ASTER Mapping and Field Validation

Ibodullo Qaraev [1 2*], Masoud Jafari Shalamzari [3] and Malihe Qaderi [4]

[1] Xinjiang Institute of Ecology and Geography, Chinese Academy of Sciences, Urumqi 830011, China

[2] Institute of Geology, Earthquake Engineering and Seismology, National Academy of Sciences of Tajikistan, Dushanbe 734017, Tajikistan

[3] Tabas Branch, Department of Environment, Tabas 9791735618, Iran

[4] South Khorasan Province Department of Environment, Department of Environment, Birjand 9717733313, Iran

Abstract The Tajik Basin holds one of Central Asia's most complete geological archives of how the Proto-Paratethys Sea retreated and gave way to continental landscapes during the Cenozoic. Yet the spatial continuity of these Paleogene–Neogene formations remains only partly understood. In this study, we combined satellite-based spectral analysis with detailed fieldwork to better map and interpret the Ganjina–Khuroson area in southwestern Tajikistan. Using Advanced Spaceborne Thermal Emission and Reflection Radiometer (ASTER) data, we applied tailored band-ratio composites (R:2/5, G:3N, B:5/6 and R:2/1, G:3N, B:5/7) to distinguish marine carbonates from continental sandstones and clays. The Maximum Likelihood Classification achieved an overall accuracy of 90.72% and a Kappa value of 0.87, demonstrating high reliability. Field spectroscopy and geological verification confirmed excellent agreement with observed lithologies. The results reveal a clear shift from fossil-rich marine limestones to oxidized continental deposits, marking the final regression of the Proto-Paratethys Sea. This integrated approach shows how multispectral data, when validated in the field, can illuminate the history of marine withdrawal and sedimentary transformation across the Tajik Basin.

1. Introduction

Satellite remote sensing has become an indispensable tool in geological investigations, offering the ability to distinguish rock types and identify mineral resources across large and often inaccessible terrains. This capability is especially valuable in regions with limited ground access or harsh environmental conditions. Numerous studies have demonstrated that satellite imagery is highly effective in discriminating lithological units and detecting key mineralogical compositions, particularly in formations dominated by carbonate minerals (Gomez et al. 2005; Rajendran and Nasir 2014; Ding, C., Liu, X., Liu, W., Liu, M., & Li, Y. (2014).; Ma and Tong 2025). These marine and continental formations, composed mainly of carbonate minerals such as calcite and dolomite,

are not only essential for geological interpretation but also hold significant economic value. Consequently, their spatial distribution, genesis, and depositional environments have long been subjects of scientific interestRemote sensing techniques, especially those employing multispectral and hyperspectral data, are widely used for mapping carbonate rocks and related mineralization. These approaches facilitate rapid, large-scale geological mapping that would otherwise be time-consuming and costly in the field (Corrie, R., Ninomiya, Y., Aitchison, J. (2011); Gad and Kusky 2007; Rockwell and Hofstra 2008; Rajendran and Nasir 2014; Özyavaş 2016 Rockwell, B.W., Hofstra, A.H. (2008)). The major advantage of remote sensing lies in its ability to capture spectral signatures that are diagnostic of particular minerals and rock types. In the field of mineral exploration, such imagery is employed to identify lithological boundaries, structural features like faults and fractures, and hydrothermal alteration zones based on their unique spectral characteristics (Crosta 1989; Chen, Zhu et al. 2016; Bahrami, Hassani et al. 2018). A range of multispectral remote sensing datasets has been employed for these purposes, and the effectiveness of these datasets has been substantiated in several studies (Corrie, R., Ninomiya, Y., Aitchison, J. (2011); Serkan Öztan and Lütfi Süzen 2011; Wahi et al. 2013; Rockwell, B.W., Hofstra, A.H. (2008); Bahrami et al. 2018).

One of the most widely used sensors for geological applications is the Advanced Spaceborne Thermal Emission and Reflection Radiometer (ASTER), launched on NASA's Terra spacecraft in December 1999. ASTER captures data in multiple spectral regions, including three bands in the visible and near-infrared (VNIR) at 15-meter spatial resolution, six bands in the short-wave infrared (SWIR) at 30-meter resolution, and five bands in the thermal infrared (TIR) at 90-meter resolution (Yamaguchi, Kahle et al. 1998; Yamaguchi and Naito 2003). The VNIR and SWIR bands are particularly effective for detecting carbonate minerals and differentiating lithological formations. These capabilities have been confirmed by numerous investigations that successfully used ASTER to detect carbonate-bearing units and associated mineralization (Gomez et al. 2005; Zhang et al. 2007; Assiri et al. 2008; Chen, Zhu et al. 2016).

This study focuses on applying ASTER VNIR and SWIR spectral data to map the Paleogene and Neogene marine and continental formations of the Ganjina-Khuroson region in the southwestern Tajik Basin. The area is characterized by a dry climate, minimal vegetation, and complex structural geology, which pose significant obstacles to detailed field mapping. Despite the region's geological importance, no prior studies have used remote sensing techniques for lithological discrimination in this context. Therefore, the primary objective of this research is to delineate the spatial distribution of the Paleogene and Neogene sedimentary sequences using ASTER data and to validate the results through comprehensive fieldwork and laboratory analysis. Digital image processing techniques, including band ratio analysis and supervised classification, were applied to the VNIR and SWIR bands. In particular, the Maximum Likelihood Classification (MLC) algorithm was employed to classify lithological units based on their spectral properties. Field campaigns were conducted to collect rock samples and verify remote sensing interpretations, supported by spectral measurements of the samples in the laboratory. This approach enabled the validation of spectral classifications and band ratio outcomes, which were also compared to existing geological maps of the area. The results demonstrate the effectiveness of ASTER data in geological mapping under challenging conditions, confirming the utility of integrated remote sensing and field-based approaches in lithological studies.

1.1. Text Background and Knowledge Gap of Proto-Paratethys Sea and Tajik Basin

The Cenozoic evolution of the Central Asian interior and the regression of the vast, shallow epicontinental Proto-Paratethys Sea are pivotal for understanding the interplay between regional paleoenvironmental change and the far-field effects of the Indo-Asia collision (Bosboom et al., 2014; Carrapa et al., 2015). Extensive research utilizing magnetostratigraphy, sedimentology, and biostratigraphy has established a broad framework for the sea's retreat, indicating a major, step-wise regression phase initiating in the Tarim Basin during the late Eocene to early Oligocene (~41-37 Ma) (Bosboom et al., 2011, 2014). Subsequent studies in the Tajik Basin, a key depocentre and final refuge of the sea, have further refined this timeline. These works link the deposition of thick evaporite sequences (e.g., the Garmabak and Gansu Formations) to the sea's final isolation and emphasize its role as one of the last retreat pathways, profoundly

influenced by the ongoing uplift of the surrounding Pamir and Tian Shan ranges (Kaya et al., 2019; Chapman et al., 2019; Ayombekov et al., 2025).

However, while these regional chronostratigraphic models are robust, a significant spatial-resolution gap persists at the local scale. The precise configuration of the Paleogene-Neogene transition—specifically, the detailed lithofacies distribution, the exact nature of contact relationships (conformable vs. unconformable), and structural controls on sedimentation during this critical interval in the southwestern Tajik Basin—remains poorly constrained. This gap is largely due to the region's complex fold-and-thrust belt geology, limited accessibility, and the inherent limitations of traditional field mapping in providing continuous, high-resolution lithological coverage (Kaya et al., 2019). Consequently, key questions regarding the paleogeographic details of the final marine retreat, the spatial variability of the ensuing continental deposition, and the potential structural segmentation of the basin margin in critical areas like the Ganjina-Khuroson region are still unresolved.

Our study directly addresses this spatial-knowledge gap. We posit that the diagnostic spectral properties of carbonate and evaporite minerals, which are direct products of the sea's retreat, can be leveraged to map this transition at an unprecedented resolution. By applying advanced ASTER multispectral data analysis, including tailored band-ratio algorithms and spectral classification, we generate a detailed lithological map. This approach provides a novel, spatially continuous perspective to test, refine, and ground-truth existing retreat models by delineating the very units that record this major paleogeographic event.

2. Materials and Methods

2.1. Study Area

The Tajik Basin is a lozenge-shaped intermountain depression situated west of the Pamirs and south of the Tian Shan, bounded by basement overthrusts and filled predominantly with Mesozoic and Cenozoic sedimentary sequences (Z., C. A 1964; Nikonov 1972; Mao and Norris 1988; Brookfield and Hashmat 2001; Bosboom et al. 2011; Chapman, Carrapa et al. 2019; Ayombekov et al. 2025). This basin represents one of the largest sediment accumulation zones in Central Asia, where deposits have resulted from the erosion of actively uplifting mountain ranges such as the Gissar, Darvaz, Pamir, and Hindu Kush, along with the erosion of underlying sedimentary complexes. The depositional processes and resulting sediment architecture are strongly influenced by tectonic, geomorphological, and lithological factors (Tang et al. 1992; Burtman and Molnar 1993; Bosboom et al. 2011). Structurally, the Tajik Basin exhibits characteristics typical of a thin-skinned fold and thrust belt, encircled by basement overthrusts which govern its internal structural configuration (Brookfield and Hashmat 2001; Chapman et al. 2019). The basin is divided into two tectonic domains: a western domain dominated by eastward-verging thrusts and folds that are synthetic to the Gissar thrust, and an eastern domain characterized by westward-verging thrusts and folds synthetic to the Pamir thrust (Nikolaev 2002; Chapman et al. 2019). Sedimentary thickness within the basin’s depocenters can reach up to 10 km, whereas in other areas it averages approximately 8 km (Brookfield and Hashmat 2001; Nikolaev 2002; Chapman et al. 2019).

Exposures of rocks older than Jurassic are absent within the basin itself, though Permian and Triassic sedimentary units occur locally along the basin margins, with thicknesses increasing toward the east and south (Nikonov 1972; Nikolaev 2002). The subtidal facies of these sequences are dominated by marine carbonate-platform and tidal-flat deposits, consisting mainly of light-colored limestones and sandstones that bear typical fossil assemblages. In contrast, the supratidal and intertidal facies are represented by lagoonal and tidal-flat deposits, including massive gypsum beds and reddish-brown gypsiferous mudstones (Markovski and Alvarez 1985; A. P. Markovski, Ministry of Geology and Conservation of the USSR, Moscow 1959; Gubin, Moscow 1960).

The Cenozoic marine sequences within the Tajik Basin are interpreted as representing a shallow-water, homoclinal ramp system (Burchette & Wright, 1992; Flügel, 2010). This low-relief depositional model is consistent with the foreland

basin setting of the region during the Paleogene (Bosboom et al., 2014; Kaya et al., 2019). The subtidal facies are dominated by inner to mid-ramp deposits, consisting primarily of bioclastic wackestones and packstones (often correlated with the light-colored, fossiliferous limestones of prior mapping: e.g., Gubin, 1960). These deposits contain a diverse assemblage of benthic foraminifera, bivalves, and gastropods (Figs. 3, 9), indicating deposition in an open-marine, normal-salinity environment largely below fair-weather wave base (Wilson, 1975; Flügel, 2010). The general absence of high-energy grain-dominated fabrics, along with a lack of observed reefal frameworks or shoal complexes with distinct cross-bedding, further supports the interpretation of a low-energy, distally-steepened ramp system rather than a rimmed platform.

In contrast, the facies association transitions basinward and upward into highly restricted environments, marking the final stages of marine occupancy. The intertidal to supratidal facies are characterized by lagoonal and sabkha deposits. These include nodular, chicken-wire, and massive gypsum beds interlayered with reddish-brown, gypsiferous mudstones (Fig. 3a, b). The presence of these evaporites is a classic indicator of deposition in arid, hypersaline settings where evaporation significantly exceeded inflow (Warren, 2006). This specific association of primary gypsum with terrigenous redbeds is a well-documented signature of terminal marine systems, often formed in salinas and coastal sabkhas along an arid coastline (Kendall & Harwood, 1996). The progression from open-marine bioclastic carbonates to these restricted evaporative facies provides a critical sedimentological record of the progressive isolation and desiccation of the Proto-Paratethys Sea in the Tajik Basin, a process driven by a combination of regional tectonic uplift and global eustatic fall (Bosboom et al., 2014; Kaya et al., 2019; Chapman et al., 2019). This facies transition is a key stratigraphic marker for correlating the regional regression event.

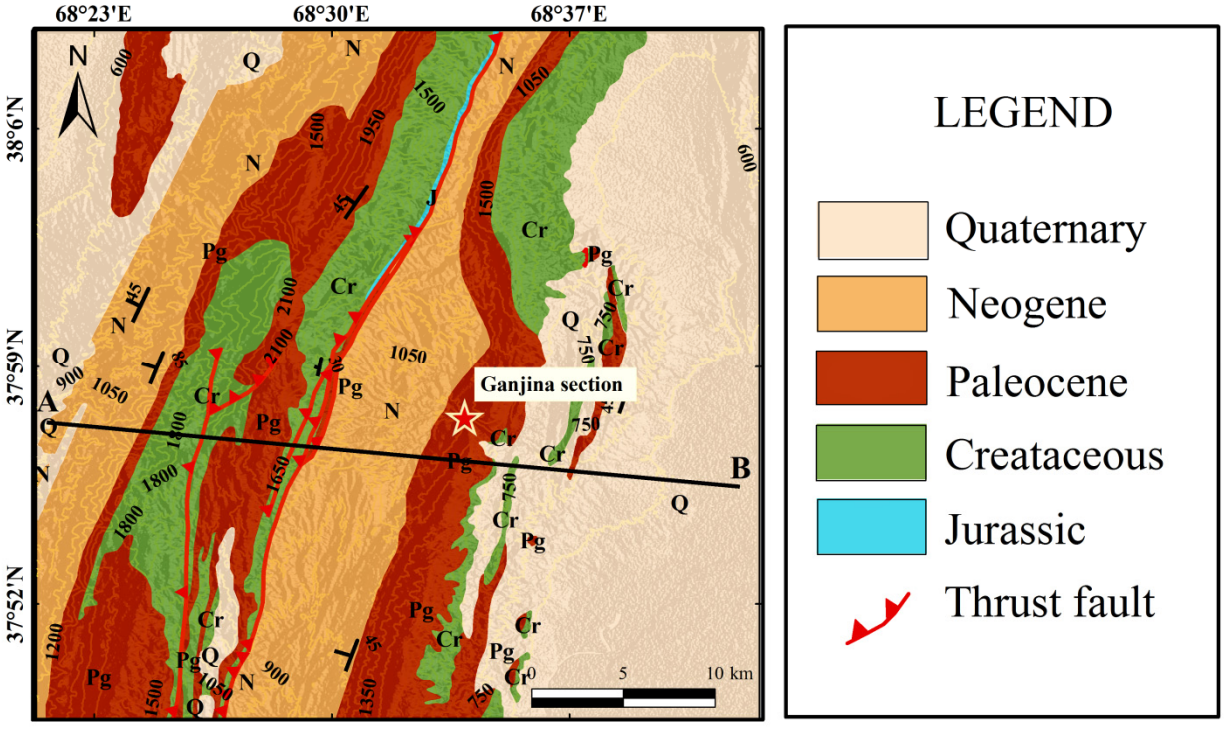

Fig. 1 A detailed geological map of the Ganjina-Khuroson area was produced through the integration of remote sensing data, field investigations, and prior geological mapping at a 1:200,000 scale (digitalized and modified after Bekker N. A. and Molchabov A. P.)

The retreat of the Proto-Paratethys Sea during the late Eocene to early Oligocene had a profound impact on the geological evolution of the Ganjina–Khuroson region. As the sea progressively withdrew toward the northwest, marine carbonate deposition gave

way to continental sedimentation dominated by fluvial and lacustrine processes. This transition resulted in a marked lithological change from thick, fossiliferous marine limestones and marls with gypsum interbeds to reddish-brown sandstones, siltstones, and mudstones of continental origin. The regression phase also led to increased siliciclastic influx derived from the uplifting Pamir and Gissar ranges, accompanied by enhanced oxidation and weathering in subaerial environments, which produced hematite-stained sediments and evaporitic horizons (Bosboom et al. 2011; Chapman et al. 2019). The Ganjina-Khuroson section (Figs. 2 and 3) is characterized by a thick sequence of stable, nodular sandstone, limestone, and gypsum, overlain by soft, multicolored slate and marl containing abundant seashell fossils. In subsequent stratigraphic layers, exposures of highly weathered shales and marls are observed, which are diagnostic of the formation. The boundary between the lower and upper parts of these formations is distinctly sharp, as evidenced by notable changes in both structural features and lithological composition (Fig. 3). Field observations reveal that limestone-rich marls, commonly exhibiting a white coloration, dominate the lithological sequences. These sequences indicate a high concentration of carbonate minerals, primarily calcite and dolomite. The rocks show signs of alteration, displaying dark brown, red, and yellow hues, often accompanied by a porous texture (Figs. 3 and 4). Calcite and dolomite are the principal carbonate minerals present, predominantly occurring within the limestone units identified during field investigations.

These changes reflect a fundamental shift in depositional energy and chemistry, marking the transformation of a shallow-marine carbonate platform into a continental foreland basin setting following the final isolation and desiccation of the Proto-Paratethys Sea (Brookfield and Hashmat 2001; Bosboom et al. 2011; Ayombekov et al. 2025). The Paleogene and Neogene carbonate and continental formations within the Ganjina-Khuroson section are generally friable. Consequently, the complex structural framework of the Tajik Basin, compounded by regional tectonic deformation such as thrust faulting, significantly impacts the geological characteristics of the study area. These tectonic features also have notable implications for the local environment and climate, as illustrated in Fig. 1 and 2.

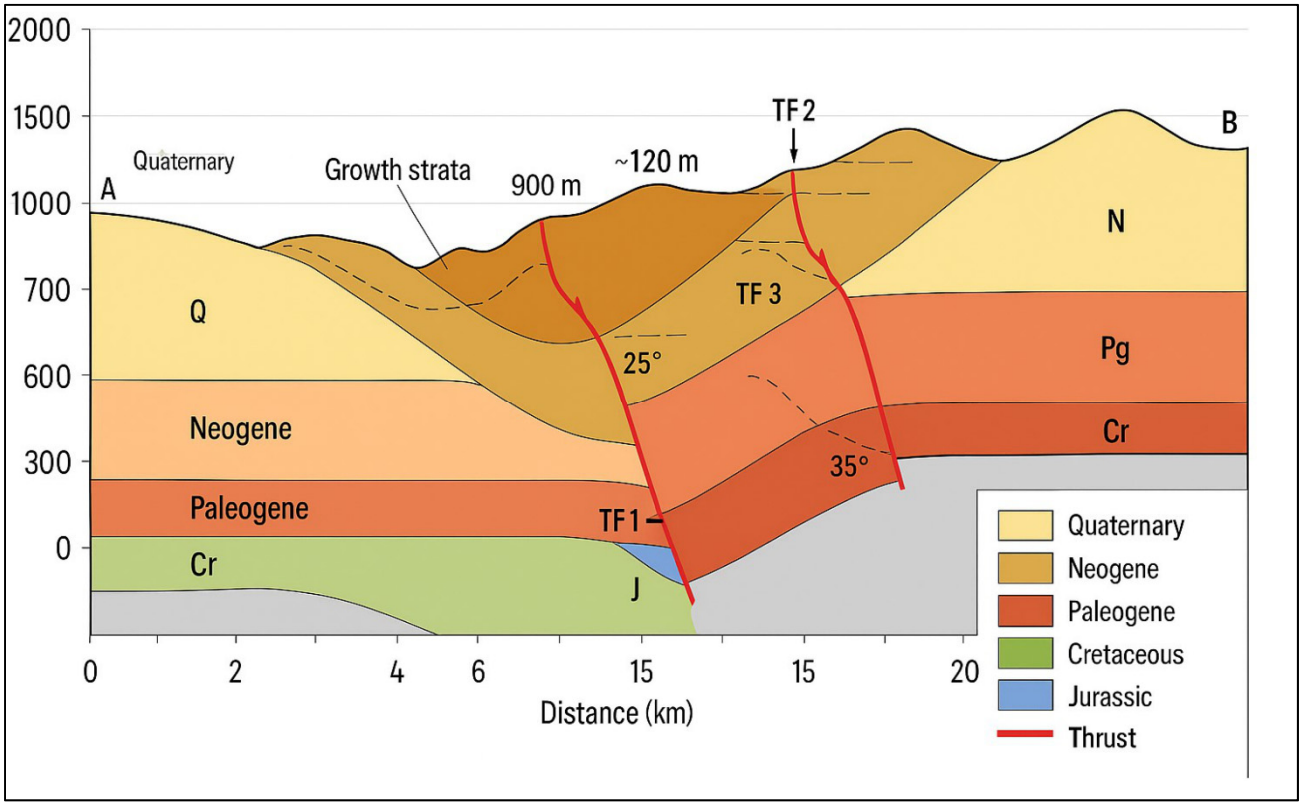

Fig. 2 Digital geological cross section of the study area (digitalized and modified after Bekker N. A and Molchabov A. P).

To this end, we conducted detailed field studies and utilized a modified geological map to construct geological cross-sections along lines A and B, enabling an in-depth analysis of the Paleogene and Neogene stratigraphic conditions in the Ganjina-Khuroson area (Figs. 1 and 2). The geological cross-section presented in Fig. 2, together with the newly modified geological map, was evaluated through remote sensing image interpretation and validated by fieldwork observations (Fig. 3).

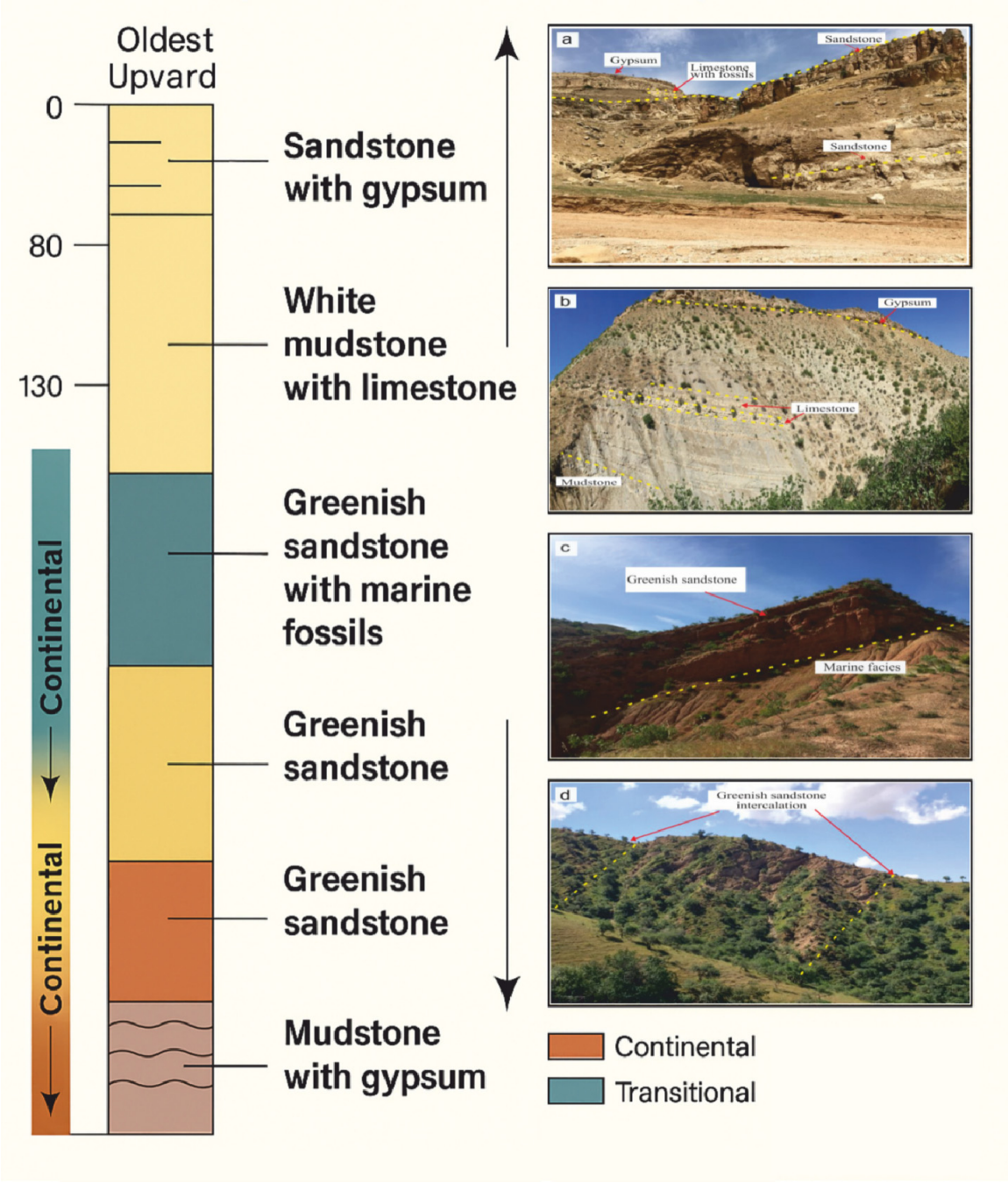

Fig. 3 Stratigraphic column summarizes the vertical facies evolution of the Ganjina–Khuroson section, integrating field photographs (a–d) to show the transition from marine to continental environments. Key stratigraphic surfaces include field views illustrate: (a) dark sandstone, limestone, and gypsum with fossils at the base; (b) white gypsum interbedded with

limestone; (c) the transition from marine greenish sandstone to continental deposits; and (d) alternating greenish sandstone and siltstone, collectively recording a regressive depositional trend.

2.2. Remote sensing data

In this study, the spectral bands of ASTER (data set AST_L1B_20181224111742_24060.HDF) were employed to map the Paleogene and Neogene formations across the entire Ganjina-Khuroson area. The ASTER Level 1B sensor radiance data, acquired on August 31, 2003, covers the study region, which is characterized by a low vegetation index. The selection of ASTER band ratios in this study was not arbitrary but based on the diagnostic spectral responses of major lithological classes in the VNIR–SWIR regions. Carbonate rocks such as limestone and dolomite show distinct absorption features near 2.33 μm (ASTER band 7) and relatively high reflectance in bands 2–5 due to overtones of CO_3^{2-} vibrations (Corrie, R., Ninomiya, Y., Aitchison, J. (2011); Rajendran and Nasir 2014). In contrast, silicate-rich and clay-bearing rocks display absorption minima in bands 6–8, corresponding to Al–OH and Mg–OH features (Gad and Kusky 2007; Chen et al. 2016). Preprocessing of the imagery was conducted using Environment for Visualizing Images (ENVI 5.3), ERDAS Imagine, and ArcGIS 10.5 software. Geometric correction was applied to align the data with the geological map of the study area at a 1:200,000 scale (WGS 1984 UTM zone 42N projection). The selection of ASTER band ratios in this study was guided by the spectral behavior of carbonate and silicate minerals across the VNIR–SWIR range. Carbonate rocks, such as limestone and dolomite, exhibit strong absorption near 2.33 μm (ASTER band 7) and high reflectance in bands 2–5, making ratios involving these bands particularly sensitive to carbonate-rich lithologies (Corrie, R., Ninomiya, Y., Aitchison, J. (2011); Gad and Kusky 2007; Rajendran and Nasir 2014). The R2/5, G3N, B5/6 and R2/1, G3N, B5/7 combinations effectively enhance contrast between carbonate and non-carbonate units by exploiting these diagnostic absorption and reflection features (Rockwell and Hofstra 2008; Özyavaş 2016; Rockwell, B.W., Hofstra, A.H. (2008)). The analysis and interpretation focused primarily on mapping Paleogene and Neogene marine carbonate and continental sequences, with emphasis on the reflectance spectra of these target formations derived from ASTER band data. Therefore, ratios such as R2/5, G3N, B5/6 and R2/1, G3N, B5/7 enhance the spectral contrast between carbonate and non-carbonate formations by exploiting these diagnostic absorption–reflection relationships. To better understand the spectral absorption characteristics of the formations, reflectance spectra of representative rock samples from the field were measured across the 0.350 to 2.500 μm wavelength range, with high spectral resolution in the short-wave infrared (SWIR) region, using an ASD FieldSpec®4 Hi-Res PIMA™ spectrometer. The ASTER Level 1B data offer a distinct advantage for lithological discrimination due to their unique combination of broad spectral coverage and moderate spatial resolution. This makes ASTER particularly valuable for geological remote sensing and lithological mapping, as it provides an optimal balance between spectral range and resolution have been validated in various geological settings—from evaporitic to siliciclastic terrains—confirming their robustness for lithological discrimination in mixed sedimentary basins like the Ganjina–Khuroson area

2.3. Preprocessing

The ASTER data (AST_L1B_20181224111742_24060.HDF) were georeferenced and subjected to atmospheric correction using the Fast Line-of-sight Atmospheric Analysis of Spectral Hypercubes (FLAASH) algorithm, followed by Post-FLAASH band math, to eliminate the spectral effects of aerosols and water vapor. To further mitigate haze effects and convert digital number (DN) values to relative reflectance, a conventional technique involving subtraction of the minimum DN value and division by the maximum DN value for each band was applied (Sabins 1987). To ensure spectral consistency and accurate boundary detection, all ASTER bands were co-registered and resampled to a common 15 m spatial resolution corresponding to the VNIR subsystem. The SWIR bands (30 m) were resampled using the nearest-neighbor algorithm to preserve original radiometric values, while the TIR bands (90 m) were excluded from lithological classification due to their coarser resolution. Prior to ratioing and classification, sub-pixel co-registration between VNIR and SWIR images was refined using ground control points and automatic image-to-image matching within ENVI 5.3, achieving a root-mean-square error (RMSE) of less than 0.5 pixels. This

procedure minimized geometric distortions that could otherwise influence spectral ratio precision and class boundary delineation (Yamaguchi et al. 1998; Gad and Kusky 2007; Rajendran and Nasir 2014; Abrams and Yamaguchi 2019). Such preprocessing steps have proven essential in earlier studies for improving lithological discrimination and ensuring reliable integration of VNIR–SWIR datasets over heterogeneous terrains (Rockwell, B.W., Hofstra, A.H. (2008); Son, Y.-S., Lee, K., Lee, S. (2022)). The minimum DN value was identified from dark pixels corresponding to water bodies such as lakes or rivers, while the maximum DN value was derived from bright pixels representing dry Salt Lake beds or exposed rock surfaces (Kavak 2005). Additionally, a novel calculation was introduced for this region to enhance the delineation of lithological cavities, facilitating clearer identification of geological elements within the study area. The region was subsequently divided into distinct rock units according to their stratigraphic ages and structural features, including faults, as summarized in Table 1. Following preprocessing, several False Color Composites (FCC) of ASTER band combinations were generated and visually assessed. The combination of RED: band 7, GREEN: band 3, and BLUE: band 1 (Fig. 4) was found to be most effective in discriminating between different lithological units and continental formations across the study area. Each false color composite integrates valuable geological, topographic, and surface roughness information, thereby enhancing lithological mapping (Ryerson and Rencz 1999, Rockwell, B.W., Hofstra, A.H. (2008), Son, Y.-S., Lee, K., Lee, S. (2022)).

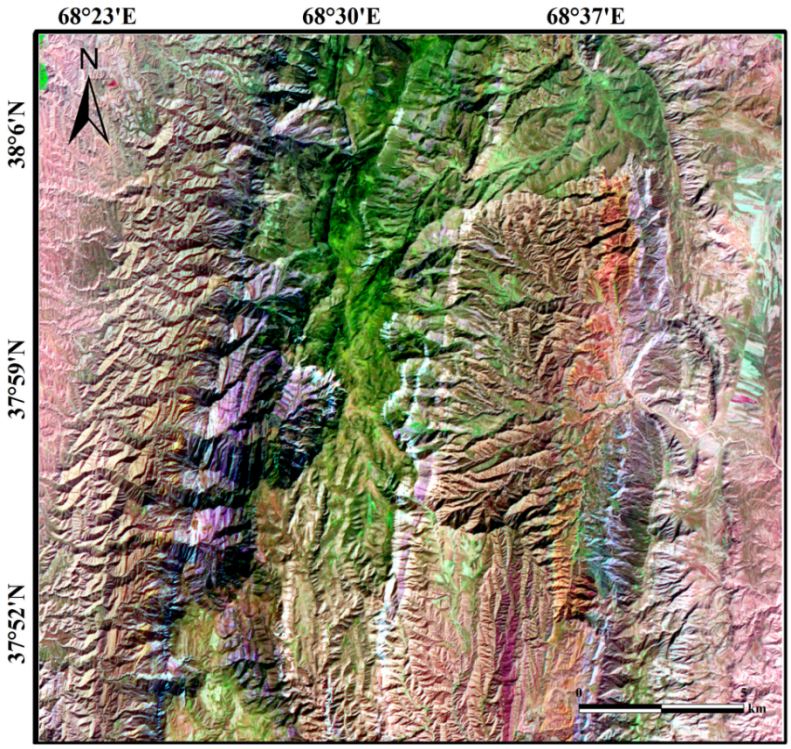

Fig. 4 False Color Composites (FCC) image 7, 3 and 1 (RED:7; GREEN:3; BLUE:1) of the study area.

Table 1. Relevant statistics of ASTER_1B bands for the study area.

Correlation	b1	b2	b3	b4	b5	b6	b7	b8	b9
Band1	1	0.97	0.89	0.8	0.8	0.8	0.8	0.8	0.72
Band2	0.97	1	0.9	0.82	0.81	0.81	0.81	0.81	0.74

Band3	0.89	0.9	1	0.76	0.68	0.69	0.68	0.68	0.61
Band4	0.8	0.82	0.76	1	0.94	0.95	0.93	0.91	0.87
Band5	0.8	0.81	0.68	0.94	1	0.99	0.99	0.98	0.91
Band6	0.8	0.81	0.69	0.95	0.99	1	0.98	0.98	0.92
Band7	0.8	0.81	0.68	0.93	0.99	0.98	1	0.99	0.91
Band8	0.8	0.81	0.68	0.91	0.98	0.98	0.99	1	0.92
Band9	0.72	0.74	0.61	0.87	0.91	0.92	0.91	0.92	1

2.4. Band ratio

Band ratio analysis is a widely recognized and effective technique for mapping different lithological units as well as alteration zones. This method involves dividing the digital number (DN) values of one spectral band by those of another, generating new relative intensity values that highlight spectral contrasts between materials (Yamaguchi and Naito 2003, San, Sumer et al. 2004, Wahi, Taj-Eddine et al. 2013). In this study, band ratios were employed as a primary tool to map the Paleogene and Neogene marine carbonate and continental sequences in the Ganjina-Khuroson section, as well as to demonstrate the potential applicability of this method in mountainous and otherwise inaccessible regions. The Paleogene and Neogene formations of marine carbonate and continental origin exhibit high spectral reflectance in ASTER bands 3 and 5 and strong absorption in bands 6 and 7. Several band ratio combinations were tested on the target outcrops, with the R2/5-G3/N-B5/6 and R2/1-G3/N-B5/7 composites identified as the most effective for lithological discrimination. Building upon previous research, multiple band ratio algorithms such as 4/7-4/6-4/10 and 4/7-3/4-2/1 (Yamaguchi et al. 2003, Kavak 2005, Gad and Kusky 2007, Serkan Öztan and Lütfi Süzen 2011) were also evaluated in RGB composites for the Ganjina-Khuroson area. Additionally, novel equations including R:1/2-G:8/1-B:9/1, R:3/1-G:5/1-B:8/1, and R:4/2-G:6/1-B:7/1 were tested for the first time. Ultimately, the R2/5-G3/N-B5/6 and R2/1-G3/N-B5/7 ratios proved most effective for discriminating the Paleogene and Neogene formations (Fig. 6 and 7). In these ratio images, marine carbonate formations appear as bright pixels due to their distinct reflectance properties, especially in band 7 (Fig. 5). Furthermore, these band ratios facilitated the differentiation of other continental lithologies within the study area. Comparison of the band ratio results with False Color Composite (FCC) images using bands 7, 3, and 1 (Fig. 4) confirmed consistent lithological discrimination, with carbonates highlighted by contrasting colors and distinct textural relief. To validate these findings, comprehensive fieldwork was undertaken, and the classification accuracy was quantitatively assessed using confusion matrix analysis in conjunction with the Maximum Likelihood Classification (MLC) algorithm applied to the Ganjina-Khuroson formations (Table 2). Under these conditions, metrics such as overall accuracy or producer/user accuracy may yield inflated results due to class prevalence effects, whereas Kappa compensates for this bias by quantifying the proportion of agreement beyond random chance (Congalton 1991; Foody 2002). Moreover, κ incorporates the full confusion matrix rather than individual class accuracies, thus offering an integrated representation of spatial and spectral consistency across all lithological classes. Although alternative indices such as the F1-score or Matthews correlation coefficient are effective in binary or highly balanced classifications, they provide limited interpretive value in complex multiclass systems typical of geological mapping (Stehman 1997; Liu et al. 2007). Therefore, in the context of this study—characterized by multiple lithological categories, varying spatial dominance, and field-verified spectral heterogeneity—the Kappa coefficient remains the most statistically rigorous and interpretable metric for evaluating classification reliability. Its high value ($\kappa = 0.87$) quantitatively confirms the strong concordance between ASTER-derived classifications and field observations, validating both the spectral methodology and geological interpretation framework.

2.5. Spectral classifier (MLC)

The spectral classification method has been effectively developed for application to both hyperspectral and multispectral remote sensing data (Manap and San 2018, Rajendran et al. 2018). In this study, the Maximum Likelihood Classification (MLC), a supervised classification technique, was applied alongside band ratio analysis to identify and validate the Paleogene and Neogene marine carbonate and continental formations based on their spectral characteristics. Field investigations provided essential geological data, and representative rock samples were analyzed for reflectance spectra using an ASD Hi-Res spectrometer. Geological maps further supported the classification process.

MLC is a widely recognized and robust spectral classification technique that enables efficient lithological mapping by evaluating the spectral similarity between image pixels and reference reflectance spectra (Abdul-Qadir 2014, Rajendran et al. 2018, Zhou, Wang et al. 2019). In this method, reference pixels—Regions of Interest (ROIs)—were selected from the image based on field observation data. The similarity between spectral signatures is calculated by determining the angle between the vectors representing the spectral data, in a space defined by the number of spectral bands.

In the present work, a comprehensive comparison was conducted between ASTER remote sensing inputs classified using band ratios and MLC to determine the most effective approach for lithological discrimination in the Ganjina-Khuroson area (Fig. 8). The classification accuracy of MLC was assessed using various input data combinations to determine the optimal configuration for identifying the spatial distribution and composition of lithological units exposed across the study area (Table 2).

2.6. Measuring spectral signature of data

To understand the spectral absorption features of the Paleogene and Neogene marine carbonate and continental formations in the Ganjina-Khuroson region, reflectance spectra of representative rock samples were measured using an ASD FieldSpec® 4 Hi-Res spectrometer. The Cenozoic marine carbonate rocks in the study area are mixed with other lithological units, making their spectral discrimination particularly challenging. Therefore, relying solely on spectral libraries such as those provided by the USGS is insufficient for accurately characterizing the spectral features of these rocks. For this reason, the spectral data of minerals and rock samples were directly measured and collected in the field. In addition, different spectral bands from the ASTER dataset were examined to support this analysis (Fig. 5a).

To better understand the absorption characteristics of marine carbonate formations, selected rock samples from the Ganjina-Khuroson section were subjected to spectral measurements. Thin sections of these samples were also prepared for petrographic analysis to investigate the mineralogical composition in detail. The ASD FieldSpec® 4 Hi-Res spectrometer, with a spectral range of 0.350 to 2.500 μm, was calibrated using a standard white reference (Zhou, Wang et al. 2019) prior to data collection. Following calibration, spectral measurements were conducted, and each sample was measured at least three times to ensure data accuracy and reproducibility (Fig. 5b). The resulting spectral curves of field samples are shown in Fig. 5b. Studying the spectral signatures of the Paleogene and Neogene marine carbonate and continental formations is crucial for accurately distinguishing and mapping their spatial distribution and geological characteristics.

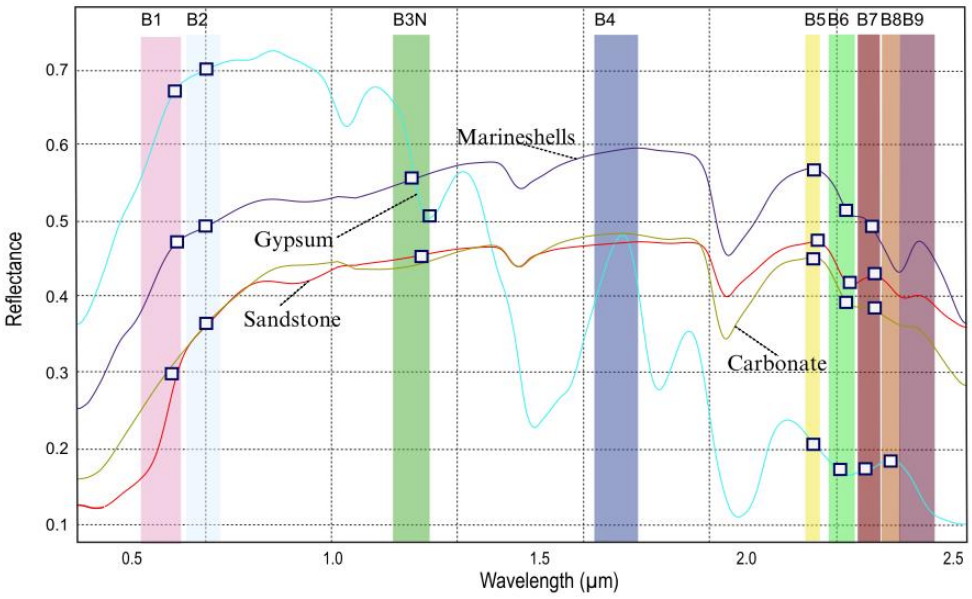

Fig. 5 Spectral curves of rock samples were measured in the wavelength range of 0.35 to 2.5 μm using an ASD FieldSpec® 4 Hi-Res spectrometer.

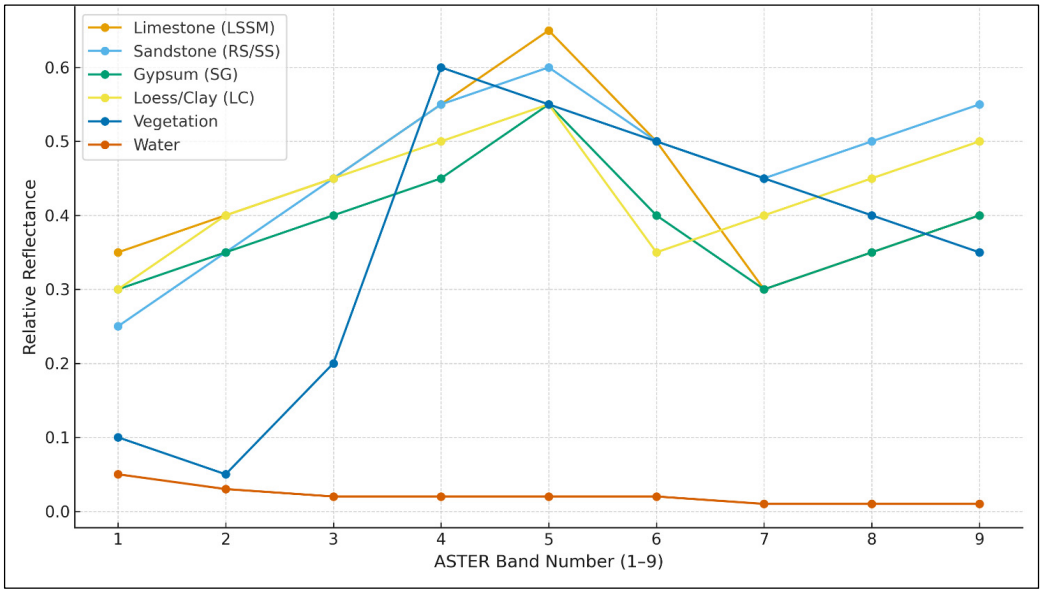

Fig. 5.1 The representative spectral signatures of the main surface materials identified in the Ganjina–Khuroson study area. Each curve shows how different lithologies and surfaces reflect solar radiation across ASTER bands 1–9, ranging from visible to shortwave infrared wavelengths. The distinct absorption features such as the carbonate trough near 2.33 μm in limestone and the hydration dips in gypsum demonstrate the clear spectral separability between rock types, vegetation, and water.

The study of spectral signatures in the Ganjina-Khuroson section is essential for distinguishing and mapping the occurrences and spatial distribution of formations. The spectral plots in Fig. 5a and 5b clearly demonstrate that carbonate

minerals exhibit distinct absorption features, which can be effectively utilized to analyze satellite spectral bands and differentiate rocks containing marine carbonate and continental formations in the Ganjina-Khuroson area.

3. Results and Discussion

In this study, the results of ASTER band analysis clearly identify the Paleogene and Neogene marine carbonate and continental formations in the Ganjina-Khuroson area. These formations appear as bright violet in the R:2/5, G:3N, B:5/6 band ratio image (Fig. 6) and greenish purple in the R:2/1, G:3N, B:7 image (Fig. 7). Carbonate-rich units, including limestone and dolomite, are represented by bright pixels, while other associated lithologies appear as dark pixels. Gypsum, clay minerals, and other continental formations show a mixture of red and white tones, enabling clear recognition and accurate delineation of their boundaries. The results demonstrate that ASTER's spectral resolution, combined with remote sensing techniques, is highly effective for mapping marine carbonate formations and detecting tectonic discontinuities. Notably, carbonate rocks, due to their spectral characteristics, are among the most suitable lithological units for remote sensing-based identification. Image interpretation and field studies also revealed distinct geomorphological features such as circular dissolution structures, valley collapses, and disappearing streams, all of which are well-correlated with stratigraphy and lithological distribution (Figs. 3 and 9).

The lithological distribution in our study area is fundamentally controlled by neotectonic processes within the active thin-skinned thrust belt. Thrust faults (Fig. 2) drive stratigraphic duplication and tectonic mixing, interleaving spectrally distinct carbonate and siliciclastic units. This creates complex outcrop patterns where ASTER's 30m resolution often captures mixed pixels, explaining classification challenges at lithological boundaries. Furthermore, the spatial distribution reflects the basin's tectonic domains: tighter carbonate exposures in the east correlate with the Pamir thrust domain, while broader Neogene sequences in the west align with the Gissar thrust domain. Thus, our spectral mapping not only identifies lithologies but also reveals how tectonic structures control surface geological expression.

The marine carbonate and continental sequences of the Ganjina-Khuroson area are easily distinguishable in the ASTER multispectral imagery, which is crucial for understanding the evolution of marine formations in the Tajik Basin. The processed images exhibit distinct relief and textures. Comparison of the two most successful band ratio combinations (R:2/5, G:3N, B:5/6 and R:2/1, G:3N, B:7) with the FCC image (bands 7, 3, 1 in RGB) shows consistent discrimination of lithological units (Figs. 6 and 7). To validate and refine these results, we applied the Maximum Likelihood Classification (MLC) algorithm, along with confusion matrix analysis. The classification achieved an overall accuracy of 90.72% and a Kappa Coefficient of 0.87 (Table 2). While multiple statistical measures exist for assessing classification accuracy, the Kappa coefficient (κ) was selected as the primary reliability index in this study because it provides a robust, chance-corrected measure of agreement that is particularly suited for lithological mapping using multispectral data. In heterogeneous geological terrains such as the Ganjina–Khuroson area, class imbalance is common—some lithological units (e.g., gypsum or loess with clay) occupy small spatial extents compared to dominant carbonate units. The best-classified units include reddish sandstone (RS), loess with clay (LC), quartz sandstones (QS), petrified marine deposits (PMD), and gypsum (G), all identified with high accuracy (Fig. 8). The User's and Producer's Accuracy metrics for the Ganjina-Khuroson section also confirm high classification reliability (Table 2). Finally, the geological map of the study area was updated based on the ASTER band ratio analysis and field survey results (Fig. 1). The use of Advanced Spaceborne Thermal Emission and Reflection Radiometer (ASTER) imagery has proven highly effective for mapping the spatial distribution of Paleogene and Neogene marine and continental lithologies. This contributes significantly to understanding the Cenozoic evolution of the Proto-Paratethys Sea in the Tajik Basin, Tajikistan.

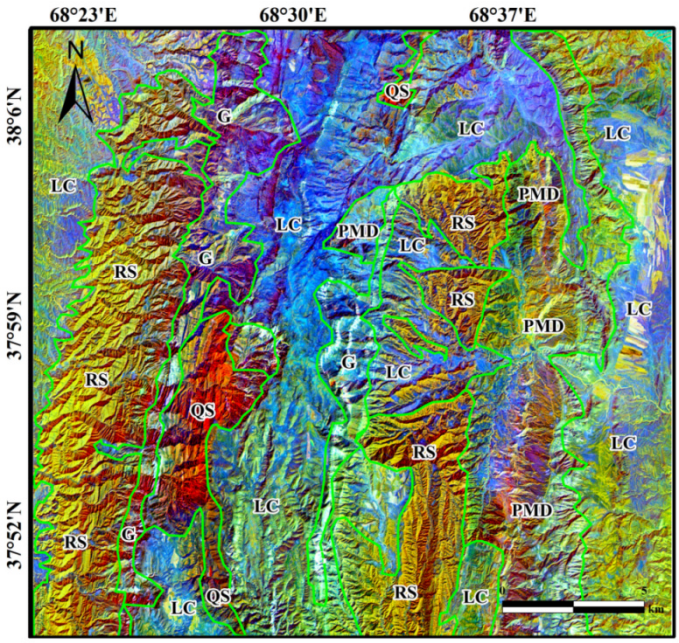

Fig. 6 Lithological classification of the Ganjina-Khuroson section. (a) ASTER Level 1B band ratio composite (R:2/5, G:3N, B:5/6) illustrating the distribution of Paleogene and Neogene marine and continental formations within the study area. Distinct lithological units are identified, including: RS – Reddish Sandstone, PMD – Petrified Marine Deposits, QS – Quartz Sandstones, LC – Loess with Clay, and G – Gypsum.

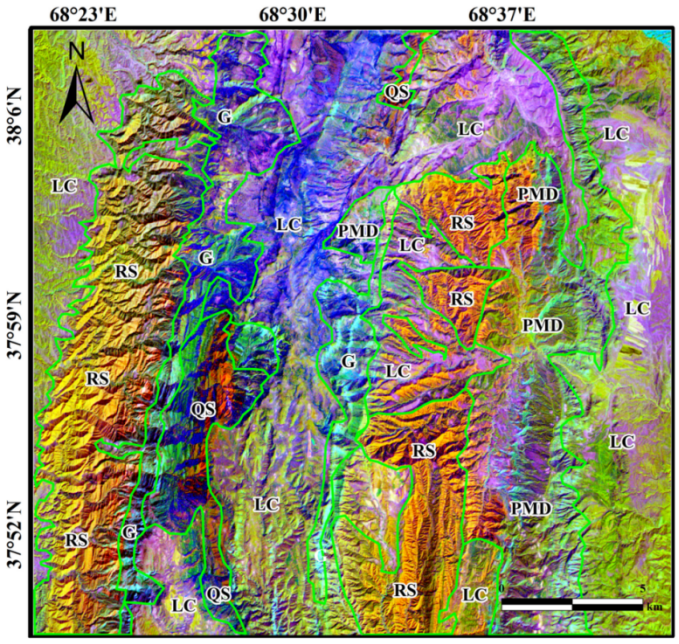

Fig. 7 Lithological classification of the Ganjina-Khuroson section. (b) ASTER Level 1B band ratio composite (R:2/1, G:3N, B:5/7) illustrating the distribution of Paleogene and Neogene marine and continental formations across the study area. Key lithological units identified include: RS – Reddish Sandstone, PMD – Petrified Marine Deposits, QS – Quartz Sandstones, LC – Loess with Clay, and G – Gypsum.

On the other hand, the Maximum Likelihood Classification (MLC) algorithm was employed to classify lithological units based on spectral information extracted from ASTER dataset images (Fig. 8). The results show a high level of lithological discrimination for the target rock units of the Ganjina-Khuroson section. Initially, the target outcrops were identified using the band ratio method, and subsequently categorized into marine carbonate and non-carbonate (continental) formations. The findings of this study demonstrate that both the spectral resolution of ASTER data and the applied remote sensing techniques are highly effective in accurately mapping these lithological units.

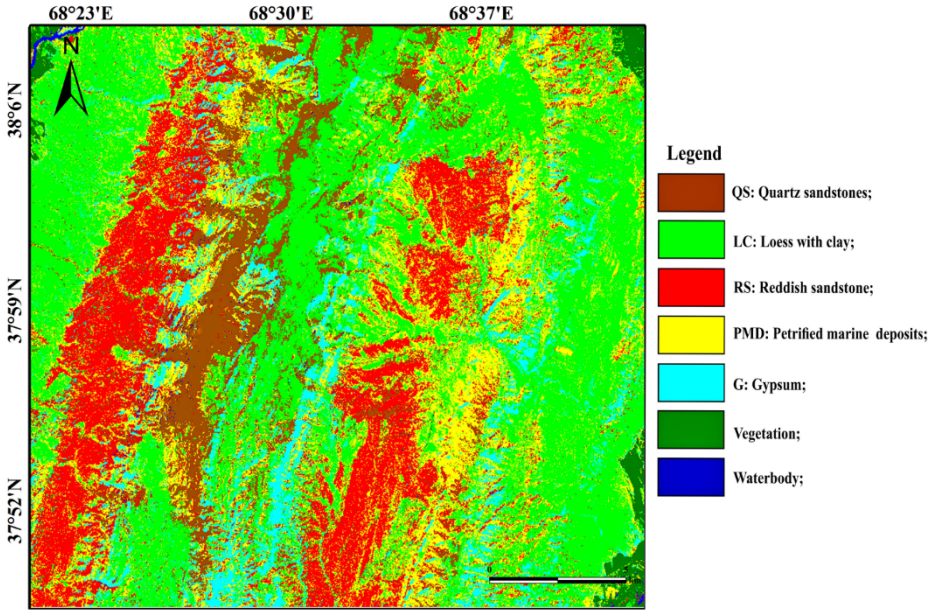

Fig. 8 The Maximum Likelihood Classification (MLC) effectively demonstrated the spatial distribution and lithological discrimination of the Ganjina-Khuroson section.

The results of the Maximum Likelihood Classification (MLC) algorithm and overall accuracy assessments indicate that the ASTER-derived datasets achieved the highest accuracy in mapping the marine and continental formations of the study area.

Table 2. Confusion matrix MLC algorithm for the Ganjina–Khuroson lithological classes.

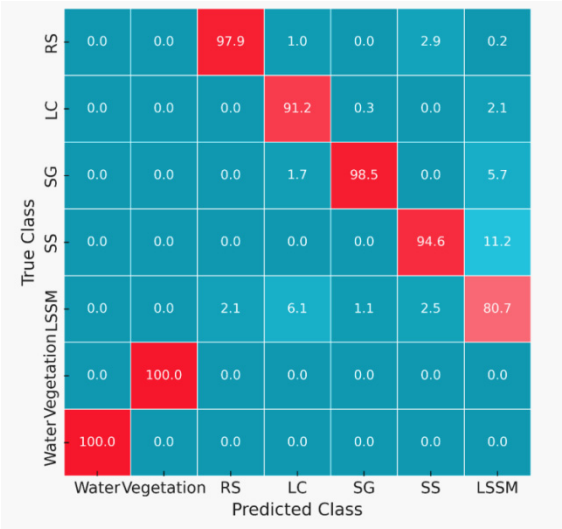

3.1. Measuring spectral signature of data

To assess the effectiveness of the ASTER spectral bands, the interpreted images were validated through field investigations aimed at detecting and delineating marine and continental formations. In the field, the Ganjina-Khuroson section appears as small seamounts (Fig. 1). Fossilized marine sediments in the study area include various species, such as different types of shells, fish teeth, and other fossil fragments ranging from large to nanoscale (Figs. 3 and 9). In hand specimens, the carbonate rocks display coral reefs filled with calcite cement, which played a significant role during the assessment.

The interpreted data were verified by field observations, where exposed lithological units were identified and their boundaries confirmed. Representative samples from various rock outcrops were collected to correlate the ASTER spectral results with ground truth (Fig. 5).

Fig. 9 Lithological distribution of the Ganjina-Khuroson area showing: (A) Sandstone; (B) Limestone with petrified marine fossils; (C) Petrified limestone with shells; (D) Mudstone with fossils and clay; (E) Siltstone with clay; (F) Mudstone with gypsum layers.

During the fieldwork, we analyzed and studied the Paleogene and Cenozoic stratigraphic sections, which reach up to 1500 m in thickness. Samples were collected along the Ganjina (GS)–Khuroson (Kh) section in the Tajik Basin (Fig. 3 and 9). The formations consist of sandstone, siltstone, limestone, mudstone, as well as fossilized marine carbonate deposits. Based on the sedimentary deposits and remote sensing results, it can be inferred that this region was once covered by a sea and later influenced by modern tectonic movements, which contributed to the formation of the large Tajik Basin.

4. Conclusion

This study transcends conventional lithological mapping by establishing a **spectral-structural framework** for deciphering the tectonic and paleoenvironmental history of the Tajik Basin. We have demonstrated that tailored ASTER band-ratio algorithms do not merely map rock types; they reveal the spatial architecture of a vanished sea. Our novel approach—specifically designed to target the Paleogene-Neogene transition—provides an unprecedented, basin-margin view of the Proto-Paratethys Sea regression, directly linking spectral signatures to the dynamics of basin closure and orogenic uplift. In this study, the Paleogene and Neogene marine and continental formations of the Ganjina-Khuroson region were mapped using ASTER multispectral bands. A novel band ratio algorithm (R2/5-G3/N-B5/6 and R-2/1, G-3N, B-5/7) was developed for the ASTER data, effectively highlighting the spectral absorption characteristics of marine carbonate and other continental formations in the study area.

The true power of this methodology lies in its ability to **bridge scales**, connecting satellite-derived spectral patterns with field-validated structural geology to show how thrust-faulting has orchestrated the final outcrop pattern of this critical stratigraphic record. Inevitably, the view through a satellite sensor has its constraints. The present work, while robust, highlights the inherent challenge of **spectral mixing** in complex tectonic terrains and the current limits of mineralogical specificity with multispectral data. These are not merely limitations but the very signposts for the next generation of geological remote sensing. Furthermore, machine learning classification, specifically the Maximum Likelihood Classification (MLC) algorithm, was applied to classify the identified outcrops in the study area. Accuracy assessment using confusion matrices showed a high Overall Accuracy = 90.72%, $\kappa = 0.87$. High UA/PA values (100%) for Vegetation and Water reflect the perfect classification of these classes for the MLC algorithm. The classification clearly delineated the Paleogene and Neogene marine carbonate and continental formations with the highest User's and Producer's accuracy. Multiple datasets were tested to optimize input parameters, achieving the best lithological classification accuracy. Notably, all algorithms identified vegetation and water bodies with a maximum accuracy of 100%. Thus, this study serves as a critical pivot point. It lays the foundational spectral-structural relationships upon which future efforts can build. The logical progression is towards a **hyperspectral and machine learning-driven paradigm**, where the sub-pixel mixtures we identified become quantifiable mineral abundances, and the structural patterns we mapped are automatically interpreted by intelligent algorithms. Our findings, therefore, not only reconstruct a key chapter in Central Asia's geological past but also provide the template for the future of tectonic geomorphology from space.

Author Contribution

I.Q.: Conceptualization, Methodology, Software, Formal analysis, Investigation, Data curation, Writing – original draft, Visualization. M.J.S.: Validation, Investigation, Resources, Writing – review & editing, Supervision, Project administration. M.G.: Writing – review & editing, Conceptualization. M.Q.: Validation, Investigation, Resources, Writing – review & editing.

Conflict of Interests

The authors declare no conflicts of interest.

Acknowledgements

The authors express their sincere gratitude to the State Scientific Institution “Institute of Geology, Earthquake Engineering and Seismology, National Academy of Sciences of Tajikistan, Dushanbe, Tajikistan” (https://igees.tj/) for their invaluable assistance and support in this research.

Reference

Abdul-Qadir, A. M., 2014, Supervised classification for lithologic discrimination in Shaikh Ibrahim Area, NW Iraq using Landsat images: Arabian Journal for Science and Engineering, v. 39, no. 1, p. 437–451, https://doi.org/10.1007/s13369-013-0911-8.

Abrams, M., and Yamaguchi, Y., 2019, Twenty years of ASTER contributions to lithologic mapping and mineral exploration: Remote Sensing, v. 11, no. 11, p. 1394, https://doi.org/10.3390/rs11111394.

Assiri, A., Alsaleh, A., and Mousa, H., 2008, Exploration of hydrothermal alteration zones using ASTER imagery: A case study of Nuqrah Area, Saudi-Arabia: Asian Journal of Earth Sciences, v. 1, no. 2, p. 77–82.

Ayombekov, Q., Chen, X., Gulayozov, M., Liu, T., Mamadbekov, F., Abdullaev, F., Yogibekov, D., Liu, H., Kabutov, Z., and Shobairi, S. O. R., 2025, Study of the impact of climate change on the runoff of the Varzob River Basin in Tajikistan: Evidence in Earth Science, v. 1, no. 02, p. 93–124, https://doi.org/10.63221/eies.v1i02.93-124.

Bahrami, Y., Hassani, H., and Maghsoudi, A., 2018, Investigating the capabilities of multispectral remote sensors data to map alteration zones in the Abhar area, NW Iran: Geosystem Engineering, p. 1–13, https://doi.org/10.1080/12269328.2018.1557083.

Bosboom, R. E., Abels, H. A., Hoorn, C., van den Berg, B. C. J., Guo, Z., and Dupont-Nivet, G., 2014, Aridification in continental Asia after the Middle Eocene Climatic Optimum (MECO): Earth and Planetary Science Letters, v. 389, p. 34–42, https://doi.org/10.1016/j.epsl.2013.12.014.

Bosboom, R. E., Dupont-Nivet, G., Houben, A. J. P., Brinkhuis, H., Villa, G., Mandic, O., Stoica, M., Zachariasse, W. J., Guo, Z., and Li, C., 2014, Timing, cause and impact of the late Eocene–early Oligocene onset of Asian aridification: Nature Geoscience, v. 7, no. 1, p. 1–6, https://doi.org/10.1038/ngeo1935.

Brookfield, M. E., and Hashmat, A., 2001, The geology and petroleum potential of the North Afghan platform and adjacent areas (northern Afghanistan, with parts of southern Turkmenistan, Uzbekistan and Tajikistan): Earth-Science Reviews, v. 55, no. 1-2, p. 41–71, https://doi.org/10.1016/S0012-8252(01)00036-8.

Burtman, V. S., and Molnar, P. H., 1993, Geological and geophysical evidence for deep subduction of continental crust beneath the Pamir: Geological Society of America, https://doi.org/10.1130/SPE281-p1.

Burchette, T. P., and Wright, V. P., 1992, Carbonate ramp depositional systems: Sedimentary Geology, v. 79, no. 1-4, p. 3–57.

Carrapa, B., DeCelles, P. G., Wang, X., Clementz, M. T., Mancin, N., Stoica, M., Kraatz, B., Meng, J., Wang, F., and Wang, H., 2015, Tectono-climatic implications of Eocene Paratethys regression in the Tajik basin of central Asia: Earth and Planetary Science Letters, v. 424, p. 168–178, https://doi.org/10.1016/j.epsl.2015.05.034.

Chapman, J. B., Carrapa, B., DeCelles, P. G., Worthington, J., Mancin, N., Cobianchi, M., Stoica, M., Wang, X., Gadoev, M., and Oimahmadov, I., 2019, The Tajik Basin: A composite record of sedimentary basin evolution in response to tectonics in the Pamir: Basin Research, v. 31, no. 6, p. 1035–1058, https://doi.org/10.1111/bre.12381.

Chen, J., Zhu, Q., Zhao, W., Sun, Z., Zhang, C., Mao, Z., and Zhao, Q., 2016, Lithological mapping using ASTER and magnetic data: A case study from Zhalute area, China: in Proceedings of the 2016 8th Workshop on Hyperspectral Image and Signal Processing: Evolution in Remote Sensing (WHISPERS), p. 1–5, https://doi.org/10.1109/WHISPERS.2016.8071803.

Corrie, R., Ninomiya, Y., and Aitchison, J., 2011, Applying ASTER spectral indices for geological mapping and mineral identification on the Tibetan Plateau: Geosphere, v. 7, no. 1, p. 276–289, https://doi.org/10.1130/GES00630.1.

Crosta, A. P., 1989, Enhancement of Landsat Thematic Mapper imagery for residual soil mapping in SW Minais Gerais State, Brazil: A prospecting case history in Greenstone belt terrain: in Proceedings of the Seventh Thematic Conference on Remote Sensing for Exploration Geology, Calgary, p. 1173–1187.

Ding, C., Liu, X., Liu, W., Liu, M., and Li, Y., 2014, Mafic-ultramafic and quartz-rich rock indices deduced from ASTER thermal infrared data using a linear approximation to the Planck function: Ore Geology Reviews, v. 60, p. 161–173, https://doi.org/10.1016/j.oregeorev.2014.01.005.

Flügel, E., 2010, Microfacies of Carbonate Rocks: Analysis, Interpretation and Application, 2nd ed.: Springer-Verlag.

Gad, S., and Kusky, T., 2007, ASTER spectral ratioing for lithological mapping in the Arabian–Nubian shield, the Neoproterozoic Wadi Kid area, Sinai, Egypt: Gondwana Research, v. 11, no. 3, p. 326–335, https://doi.org/10.1016/j.gr.2006.02.010.

Gomez, C., Delacourt, C., Allemand, P., Ledru, P., and Wackerle, R., 2005, Using ASTER remote sensing data set for geological mapping in Namibia: Physics and Chemistry of the Earth, Parts A/B/C, v. 30, no. 1-3, p. 97–108, https://doi.org/10.1016/j.pce.2004.08.042.

Kavak, K., 2005, Recognition of gypsum geohorizons in the Sivas Basin (Turkey) using ASTER and Landsat ETM+ images: International Journal of Remote Sensing, v. 26, no. 20, p. 4583–4596, https://doi.org/10.1080/01431160500185607.

Kaya, M. Y., Dupont-Nivet, G., Proust, J. N., Roperch, P., Bougeois, L., Meijer, N., Frieling, J., Fioroni, C., Özkan Altıner, S., and Vandenberghe, J., 2019, Paleogene evolution and demise of the proto-Paratethys Sea in Central Asia (Tarim and Tajik basins): Role of intensified tectonic activity at ca. 41 Ma: Basin Research, v. 31, no. 3, p. 461–486, https://doi.org/10.1111/bre.12330.

Leith, W., and Alvarez, W., 1985, Structure of the Vakhsh fold-and-thrust belt, Tadjik SSR: Geologic mapping on a Landsat image base: Geological Society of America Bulletin, v. 96, no. 7, p. 875–885, https://doi.org/10.1130/0016-7606(1985)96<875:SOTVFB>2.0.CO;2.

Ma, Q., and Tong, Q., 2025, Study on reservoir characteristic differences between the Late Triassic Yanchang Formation and Early Jurassic Yan'an Formation in Ordos Basin: A case study from Zhenbei Oilfield in southwestern margin: Evidence in Earth Science, v. 1, no. 01, p. 73–92, https://doi.org/10.63221/eies.v1i01.73-92.

Mao, S., and Norris, G., 1988, Late Cretaceous–early Tertiary Dinoflagellates and Acritarchs from the Kashi Area, Tarim Basin, Xinjiang Province, China: Life Sciences Miscellaneous Publications, Royal Ontario Museum.

Markovski, A. P., 1959, Geology of USSR, Vol. 45: The Tajik Soviet Union, Part 1: Ministry of Geology and Conservation of the USSR.

Nikolaev, V., 2002, Afghan-Tajik depression: Architecture of sedimentary cover and evolution: Russian Journal of Earth Sciences, v. 4, no. 6, p. 405–420.

Nikonov, A., 1972, To the substantiation of stratigraphy of upper plated and Quarterly deposits of Afghan-Tajik Depression: Bulletin of the Quaternary Commission, v. 39, p. 45–52.

Rajendran, S., and Nasir, S., 2014, ASTER spectral sensitivity of carbonate rocks: Study in Sultanate of Oman: Advances in Space Research, v. 53, no. 4, p. 656–673, https://doi.org/10.1016/j.asr.2013.11.047.

Rajendran, S., Nasir, S., El-Ghali, M., Alzebdah, K., Al-Rajhi, A. S., and Al-Battashi, M., 2018, Spectral signature characterization and remote mapping of Oman exotic limestones for industrial rock resource assessment: Geosciences, v. 8, no. 4, p. 145, https://doi.org/10.3390/geosciences8040145.

Rockwell, B. W., and Hofstra, A. H., 2008, Identification of quartz and carbonate minerals across northern Nevada using ASTER thermal infrared emissivity data—Implications for geologic mapping and mineral resource investigations in well-studied and frontier areas: Geosphere, v. 4, no. 1, p. 218–246, https://doi.org/10.1130/GES00126.1.

Ryerson, R. A., and Rencz, A. N., eds., 1999, Manual of Remote Sensing, Remote Sensing for the Earth Sciences, Vol. 3: John Wiley & Sons.

Sabins, F. F., 1987, Remote Sensing: Principles and Interpretation, 2nd ed.: W. H. Freeman and Company.

San, B., Sumer, E., and Gurcay, B., 2004, Comparison of band ratioing and spectral indices methods for detecting alunite and kaolinite minerals using ASTER data in Biga region, Turkey: The International Archives of the Photogrammetry, Remote Sensing and Spatial Information Sciences, v. 35, no. B7, p. 621–625.

Serkan Öztan, N., and Lütfi Süzen, M., 2011, Mapping evaporate minerals by ASTER: International Journal of Remote Sensing, v. 32, no. 6, p. 1651–1673, https://doi.org/10.1080/01431160903586799.

Son, Y.-S., Lee, K., and Lee, S., 2022, Application of ASTER data for differentiating carbonate minerals: Distinguishing magnesite, dolomite, and calcite using ASTER SWIR data: Remote Sensing, v. 14, no. 1, p. 181, https://doi.org/10.3390/rs14010181.

Wahi, M., Taj-Eddine, K., and Laftouhi, N., 2013, ASTER VNIR & SWIR band enhancement for lithological mapping—a case study of the Azegour Area (Western High Atlas, Morocco): International Journal of Engineering Research & Technology, v. 2, no. 12, p. 2278–0181.

Yamaguchi, Y., and Naito, C., 2003, Spectral indices for lithologic discrimination and mapping by using the ASTER SWIR bands: International Journal of Remote Sensing, v. 24, no. 22, p. 4311–4323, https://doi.org/10.1080/01431160110070320.

Yamaguchi, Y., Kahle, A. B., Tsu, H., Kawakami, T., and Pniel, M., 1998, Overview of advanced spaceborne thermal emission and reflection radiometer (ASTER): IEEE Transactions on Geoscience and Remote Sensing, v. 36, no. 4, p. 1062–1071.

Zhang, X., Pazner, M., and Duke, N., 2007, Lithologic and mineral information extraction for gold exploration using ASTER data in the south Chocolate Mountains (California): ISPRS Journal of Photogrammetry and Remote Sensing, v. 62, no. 4, p. 271–282, https://doi.org/10.1016/j.isprsjprs.2007.04.004.

Zhou, G., Wang, H., Sun, Y., Shao, Y., and Yue, T., 2019, Lithologic classification using multilevel spectral characteristics: Journal of Applied Remote Sensing, v. 13, no. 1, p. 016513, https://doi.org/10.1117/1.JRS.13.016513.